

Lawrence Berkeley National Laboratory

LBL Publications

Title

Two-Dimensional Titania: Structures and Properties Predicted by First Principle Calculation

Permalink

<https://escholarship.org/uc/item/5k9296c6>

Journal

The Journal of Physical Chemistry C, 122(40)

ISSN

1932-7447

Authors

Wang, Liang
Wei, Dongshan
Kang, Shuai
et al.

Publication Date

2018-10-11

DOI

10.1021/acs.jpcc.8b05412

Peer reviewed

See discussions, stats, and author profiles for this publication at: <https://www.researchgate.net/publication/327525867>

Two-Dimensional Titania – Structures and Properties Predicted by First Principle Calculation

Article in *The Journal of Physical Chemistry C* · September 2018

DOI: 10.1021/acs.jpcc.8b05412

CITATIONS

9

READS

167

5 authors, including:



Liang Wang

13 PUBLICATIONS 250 CITATIONS

[SEE PROFILE](#)



Dongshan Wei

Dongguan University of Technology

119 PUBLICATIONS 1,114 CITATIONS

[SEE PROFILE](#)



Yuping Shi

University of Oxford

22 PUBLICATIONS 128 CITATIONS

[SEE PROFILE](#)

Some of the authors of this publication are also working on these related projects:



Multi-scale investigation of interface dominated multiferroic nanostructures (IDMNS) and exploration of potential applications [View project](#)



THz Near-field Microscope [View project](#)

Two-Dimensional Titania: Structures and Properties Predicted by First Principle Calculation

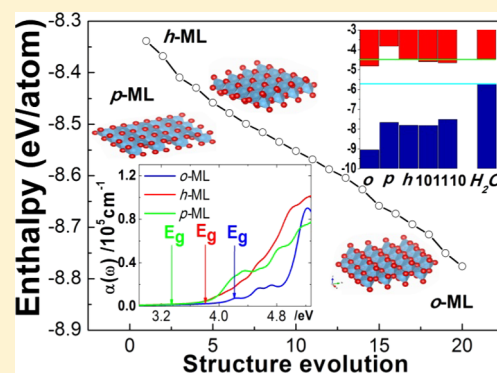
Liang Wang,^{*,†,‡,§} Dongshan Wei,[†] Shuai Kang,^{†,‡} Xiong Xie,^{†,‡} and Yuping Shi[§]

[†]Chongqing Institute of Green and Intelligent Technology, Chinese Academy of Sciences, 266 Fangzheng Avenue, ShuiTu Technology Development Zone, Beibei District, Chongqing 400714, P. R. China

[‡]Chongqing Key Laboratory of Multi-Scale Manufacturing Technology, Chongqing Institute of Green and Intelligent Technology, Chinese Academy of Sciences, Chongqing 400714, P. R. China

[§]Department of Mechanical and Aerospace Engineering, The Hong Kong University of Science and Technology, Kowloon, Hong Kong

ABSTRACT: Material innovations, especially in classic semiconductor materials such as titania, are expected and more and more accelerated by ab initio design for their wide applications. For better realization in laboratory, feasible stability of structures in ambient temperature and pressure should be prior to the structure–property relationship study. However, there is discrepancy between experiments and ab initio calculations about how the freestanding two-dimensional TiO₂ exists. Herein, by the structural search method with the first principles evolution algorithm, the stable freestanding monolayers (MLs) were found to be composed by octahedral, hexahedral, or pentahedral Ti–O block (o-ML, h-ML, or p-ML) with nonplanar structure, where o-ML is right the lepidocrocite type found experimentally. Meanwhile, novel structure-dependent properties mainly due to quantum-confine effects were investigated and the abnormal optical absorption, better properties of insulation, and redox in photocatalysis were found for these titania sheets.



1. INTRODUCTION

Titania are widely studied for their versatile structures, properties, and applications in dielectric,^{1–3} photovoltaic,⁴ photolysis,^{5,6} etc. By now, many common titania phases and structures have been explored, hence one of the mining directions has been toward some extreme conditions like high pressure in recent years.^{7,8} Meanwhile, novel properties are expected for two-dimensional (2D) nanostructured TiO₂ due to surface effects, size effects, quantum-confinement effects, etc.^{9,10} Nevertheless, feasible properties may be easily designed by ab initio methods with stability of structures in ambient temperature and pressure prior to the structure–property relationship study. By first principle calculation, oxide freestanding monolayers (MLs) of II–VI (Be, Mg, Ca, Sr, Ba, Zn, Cd, and Hg),¹¹ aluminum,¹² and copper,¹³ which exist whether as a perfect planar honeycomb or a low-buckled layer, and molybdenum¹⁴ and vanadium,¹⁴ which are nonplanar, were predicted and investigated. TiO₂ nanosheet with organic dye and nanosheet/graphene bilayers based on anatase (101) and (001) orientation were proposed for higher photoresponsivity in GW and density functional theory (DFT) calculation.^{4,15} However, the most common two-dimensional (2D) TiO₂ nanosheets have been separated from anatase by ion-intercalation and exfoliation method,^{16,17} whose structure is lepidocrocite type,^{1,18–23} indicating the gap between experiment and theory; the prediction of two-dimensional titania by pure ab

initio method is still a challenge. Meanwhile, the novel properties relevant with nanostructure and physics behind them attract many researchers' attentions.

Herein, we present the result of searching the freestanding monolayer by ab initio structure prediction method and properties of optics and photocatalysis studied by first principle calculation, where stable monolayers formed by Ti–O hexahedron (β phase) and pentahedron (γ phase) were found beyond proving in lepidocrocite phase (α phase) as the lowest-enthalpy freestanding structure of 2D TiO₂. Moreover, these titania sheets were found to be phononic crystal candidate materials and wide band gap semiconductors with band gaps larger than 3 eV. Better insulation properties are expected for the layered structures compared to those of bulk TiO₂. Abnormal optical absorption was observed, and the strongest reducibility and oxidizability in photocatalysis were found in h-ML and o-ML, respectively.

2. METHODS

2.1. Structure Prediction. USPEX code²⁴ with evolution algorithm implemented was employed for low-enthalpy 2D structure searching. The population size and the number of

Received: June 6, 2018

Revised: August 23, 2018

Published: September 7, 2018

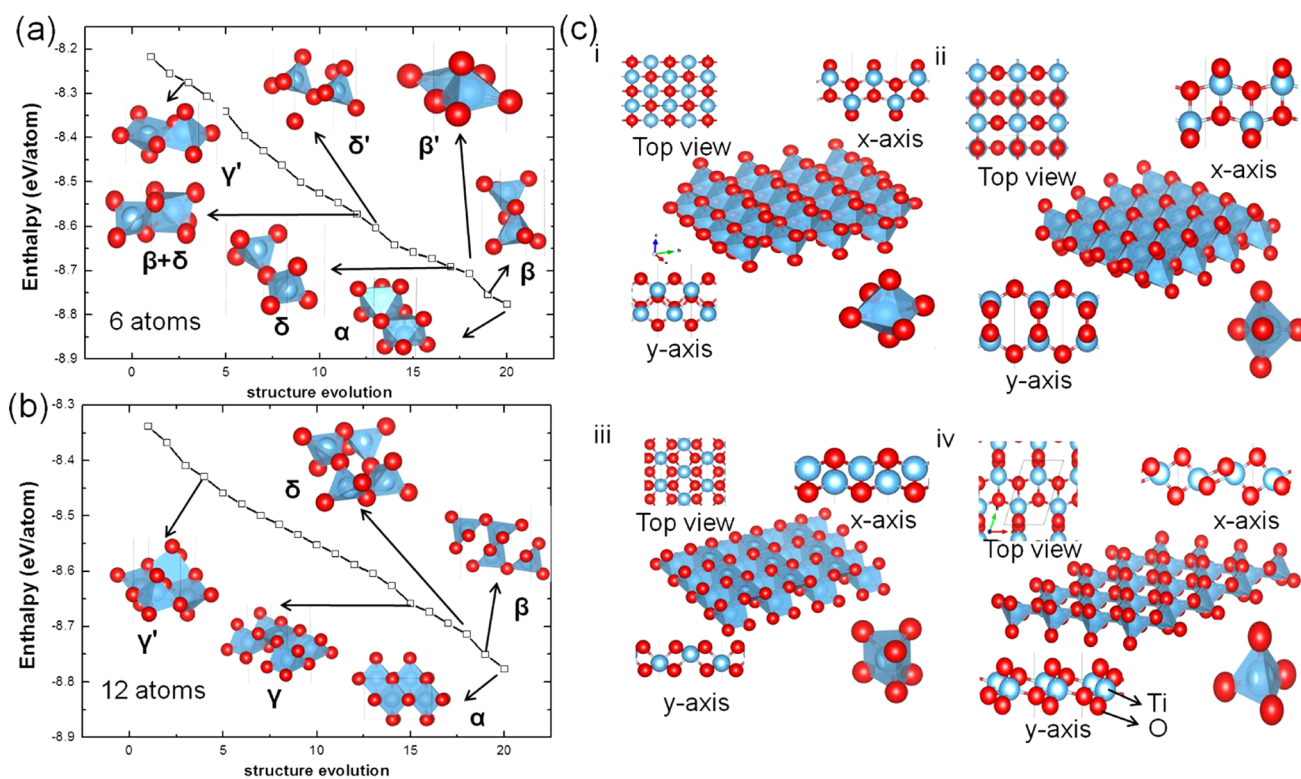


Figure 1. Evolution of a good structure with enthalpy. (a) 6 atoms; (b) 12 atoms, Ti/O = 1:2; (c) the lowest-enthalpy 2D TiO₂ monolayers with different Ti–O polyhedral blocks; the view from top and *x*/*y* axis direction and polyhedral view and their basic blocks are displayed: (i) lepidocrocite type with octahedral block (α phase), (ii) monolayer with hexahedral block (β phase), (iii) monolayer with pentahedral block (γ phase), and (iv) monolayer with tetrahedral block (δ phase).

Table 1. Optimized Structure of the Four Different 2D TiO₂ with Single Polyhedral Block^a

phase	α -2D-TiO ₂	β -2D-TiO ₂	γ -2D-TiO ₂	δ -2D-TiO ₂
space group	<i>Pmnm</i>	<i>Pmma</i>	<i>Pmnm</i>	<i>Pmc2₁</i>
<i>a</i> (Å)	3.0276	3.8634	5.1014	3.2332
<i>b</i> (Å)	3.7657	3.2582	3.0158	5.5380
<i>c</i> (Å)	18.685	16.4953	15.541	17.597
Wyckoff position	Ti 2a (0, 0, 0.54503) O 2b (0.5, 0, 0.48011) O 2b (0.5, 0, 0.58644)	Ti 2f (0.25, 0.5, 0.57998) O 2e (0.75, 1.0, 0.36138) O 2f (0.75, 0.5, 0.55016)	Ti 2a (0, 0, 0.47137) O 4f (0.23562, 0.5, 0.42653) O 2a (0, 0.77167, 0.64168)	Ti 2b (0.5, 0.32397, 0.42157) O 2b (0.5, 0.13586, 0.53269)
enthalpy (eV/atom)	−8.776	−8.754	−8.658	−8.692
thickness (Å)	4.330	4.178	1.990	2.762

^aThickness denotes the distance between atoms with the Cartesian *z* component maximum and minimum.

generation were set to be 40 and 20, respectively. For structure prediction, all initial structures are random, i.e., without seed structure specified. For simplicity, the atom ratio was set to 1:2 (Ti/O) to avoid defects. A double vacuum slab model with 15 Å vacuum was specified to avoid interaction between 2D TiO₂ layers.²¹ The required structure optimizations were performed by Vienna ab initio simulation package (VASP) code^{25,26} with projector-augmented wave (PAW)²⁷ method for potentials, where Ti 3d²4s² and O 2s²2p⁴ electrons were considered.

2.2. DFT Calculation. The structure optimization, energy, band structure, and optical parameters reported here are based on DFT calculation in the frame of plane wave-pseudopotential²⁸ implemented in VASP code. The ultrasoft Perdew–Burke–Ernzerhof (PBE) pseudopotential in general gradient approximation²⁹ was chosen for electronic exchange and correlation interaction. The plane wave cutoff energy was set to 600 eV, and the spacing of *k*-points in the Brillouin zone was set to 0.02 Å^{−1} in the Monkhorst–Pack scheme³⁰ to make sure

of the convergences of energy ($\Delta E < 2 \times 10^{-5}$ eV) and force ($\Delta F < 2 \times 10^{-4}$ eV/Å) upon structure relaxation. For precise band structure and optical calculation, the hybrid Heyd–Scuseria–Ernzerhof functional (HSE06)^{31,32} was used. The plane wave cutoff energy, energy convergence threshold, and *k*-point grid are 600 eV, 1×10^{-8} eV, and $10 \times 10 \times 1$, respectively.

2.3. Ab Initio Molecular Dynamics (AIMD) Simulation. Thermal stability of the configuration in room temperature (300 K) was checked by AIMD simulation implemented in VASP code. For each configuration, a $3 \times 3 \times 1$ supercell was used. PAW method, PBE functional, and NVT ensemble were chosen for simulation. The temperature was controlled by the Nosé–Hoover method,³³ and the time step was set to 1 fs.

2.4. Phonon Spectrum Calculation. Phonon calculation was done by density functional perturbation theory (DFPT)²⁸ code implemented in Quantum ESPRESSO.³⁴ PBE of ultrasoft PAW potential was chosen for electronic exchange and correlation interaction in self-consistent field (SCF)²⁶ calcu-

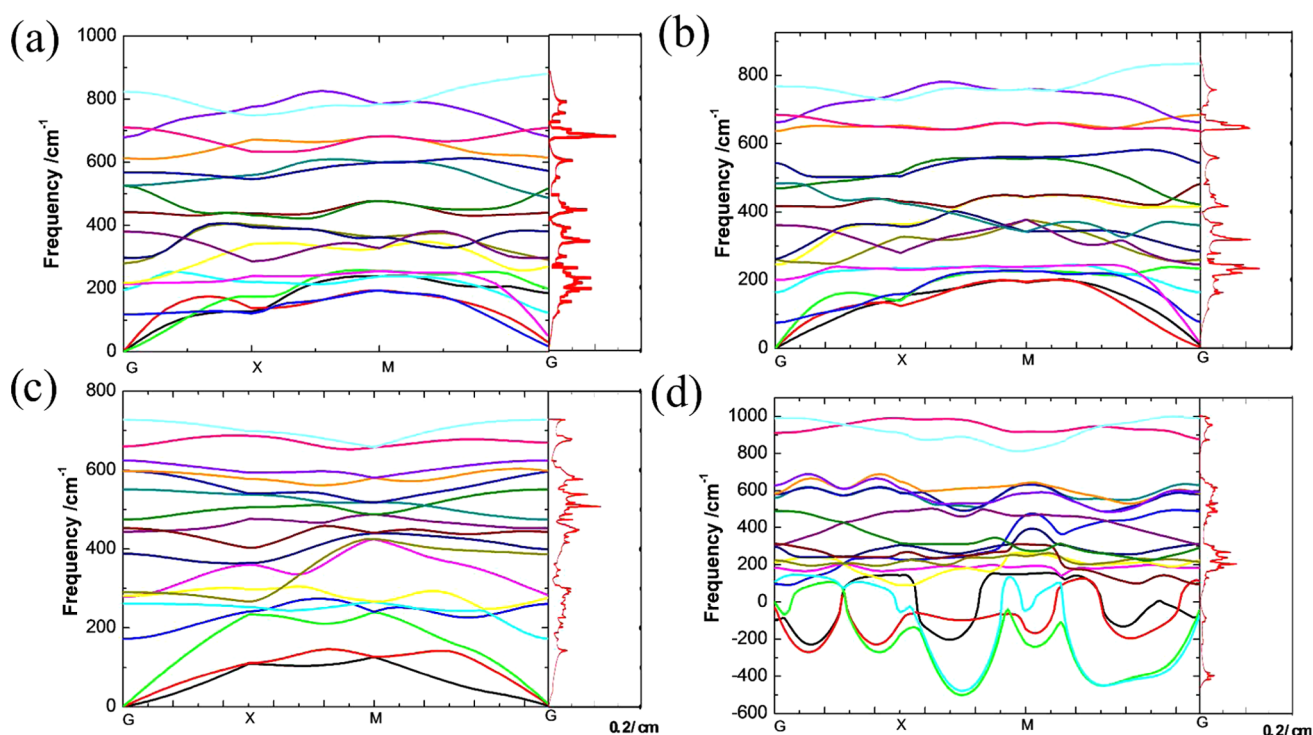


Figure 2. Phonon dispersion curve and density of state (PhDOS) of TiO_2 monolayers: (a) o-ML, α phase; (b) h-ML, β phase; (c) p-ML, γ phase; and (d) t-ML, δ phase.

Table 2. Phonon Mode and Frequencies at the Center of the Brillouin Zone and IR or Raman Activity of TiO_2 Monolayers^{a,b}

α -2D- TiO_2			β -2D- TiO_2			γ -2D- TiO_2			δ -2D- TiO_2		
mode	freq	activity	mode	freq	activity	mode	freq	activity	mode	freq	activity
B_{2u}	0	I	B_{3u}	0	I	A'	0	I + R	A	-96.22	I + R
B_{1u}	0	I	B_{2u}	0	I	A'	0	I + R	A	-27.61	I + R
B_{3u}	0	I	B_{1u}	0	I	A''	0	I + R	A	-0.17	I + R
B_{2g}	114.29	R	B_{2g}	75.31	R	A'	172.06	I + R	A	95.38	I + R
B_{3g}	168.36	R	B_{3g}	164.44	R	A'	261.32	I + R	A	109.93	I + R
B_{2u}	230.35	I	B_{2g}	197.17	R	A''	278.83	I + R	A	184.05	I + R
B_{3u}	231.95	I	B_{2u}	240.62	I	A''	281.15	I + R	A	215.47	I + R
B_{3g}	258.46	R	A_g	245.95	R	A'	289.6	I + R	A	225.26	I + R
A_g	286.66	R	B_{3g}	261.09	R	A'	387.87	I + R	A	296.93	I + R
B_{2g}	387.27	R	B_{3u}	360.71	I	A''	443.52	I + R	A	307.42	I + R
A_g	445.76	R	B_{2u}	399.92	I	A'	452.23	I + R	A	313.50	I + R
B_{2u}	496.84	I	B_{1u}	417.3	I	A''	460.77	I + R	A	490.31	I + R
B_{3u}	531.02	I	B_{2g}	471.59	R	A''	474.3	I + R	A	560.73	I + R
B_{2g}	545.65	R	B_{3u}	483.13	I	A'	550.9	I + R	A	580.73	I + R
B_{1u}	580.87	I	A_g	547.66	R	A'	596.9	I + R	A	583.32	I + R
B_{3g}	706.35	R	A_g	636.83	R	A'	605.81	I + R	A	628.37	I + R
A_g	718.04	R	B_{3g}	683.84	R	A'	624.33	I + R	A	910.75	I + R
B_{1u}	720.43	I	B_{1u}	695.87	I	A'	731.51	I + R	A	988.99	I + R

^a(a) o-ML, α phase; (b) h-ML, β phase; (c) p-ML, γ phase; and (d) t-ML, δ phase. ^bI and R indicate infrared activity and Raman activity, respectively.

lation. Energy cutoffs are 60 and 780 Ry for the wave function and charge density and the k -point grids for SCF and lattice-dynamical matrices are $12 \times 12 \times 2$ and $6 \times 6 \times 1$, respectively. Structures were relaxed to an energy convergence threshold and ionic force of 1×10^{-10} Ry and 1×10^{-8} Ry/b, respectively, before lattice-dynamical matrices calculation.

3. RESULTS AND DISCUSSION

Figure 1a,b shows the evolution of a good structure of titania sheet with enthalpy from high to low during which the enthalpy varies from -8.219 to -8.776 eV/atom. It shows the Ti–O polyhedrons whether tetrahedral, pentahedral, hexahedral, or octahedral are the basic blocks for building two-dimensional TiO_2 . Generally, the structure with mixing of n -polyhedron ($n = 4, 6$), e.g., configuration 12 in Figure 1a ($\beta + \delta$ phase), or single polyhedron without coedge, e.g., configuration 1 (δ'' phase) in

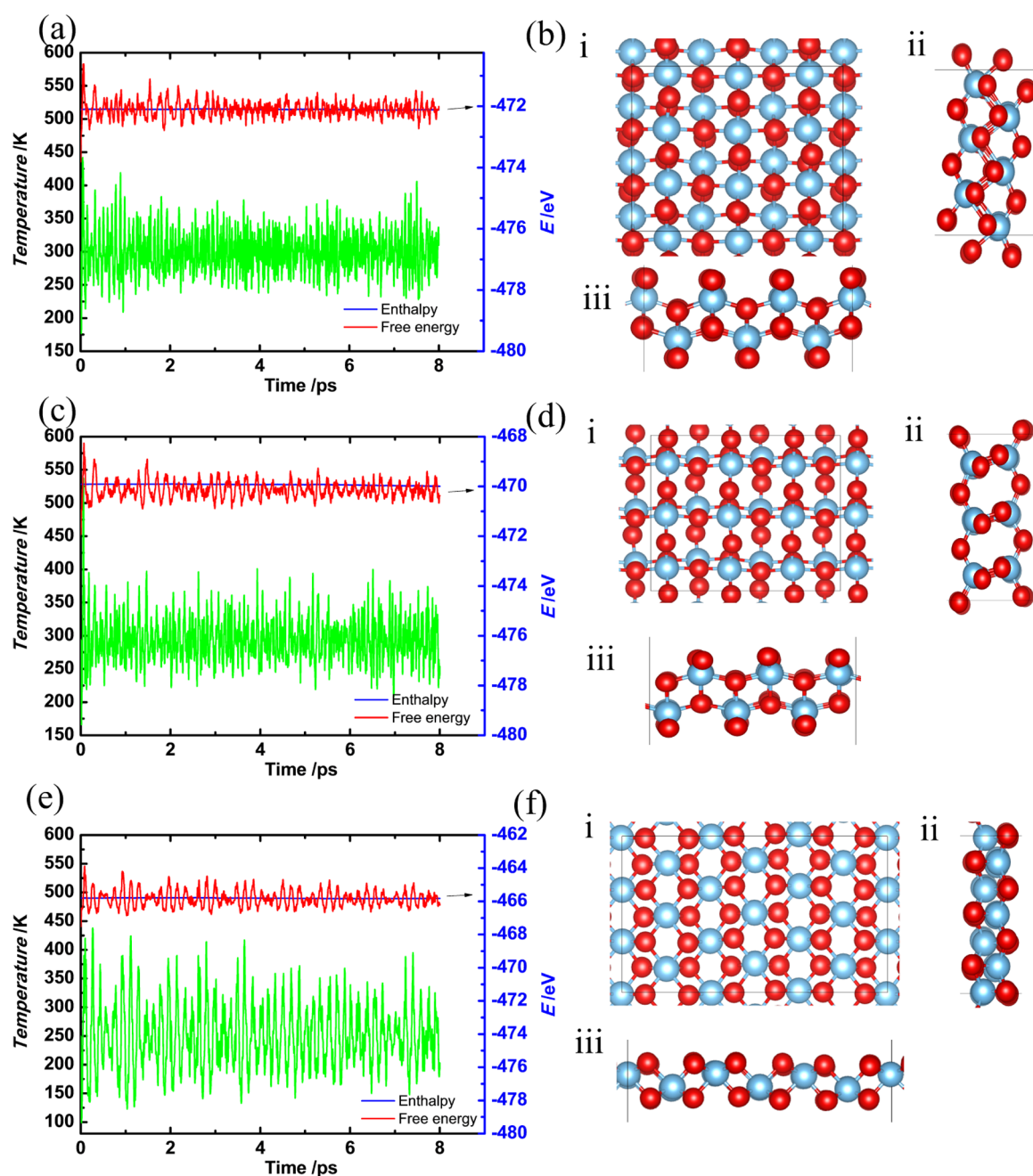


Figure 3. Molecular dynamics simulation of TiO_2 monolayer at 300 K, the fluctuation of temperature, enthalpy, and free energy in the final configuration. (a, b) o-ML, α phase; (c, d) h-ML, β phase; and (e, f) p-ML, γ phase. The red balls represent the oxygen atoms, whereas the cyan balls represent the titanium atoms.

Figure 1a, is not energetically favorable. The four TiO_2 monolayer structures composed by α , β , γ , and δ phase are listed in Figure 1c and Table 1. They are all formed by unique polyhedral block. The coordination numbers of Ti in the four titania sheets are 6, 5, 6, and 4, respectively, indicating the Ti–O bonds are ionic. The space group and enthalpy of the four structures are $Pmmm$, -8.776 eV/atom; $Pmma$, -8.754 eV/atom; $Pmnn$, -8.658 eV/atom; and $Pmc2_1$, -8.692 eV/atom, respectively. Compared with previous proposed structures,^{4,15} O termination and no dangling bonds are two main features for predicted structures. From energy perspective, these features are more helpful for lowering system enthalpy. Also, they indicate a relatively inert surface as a price of stability.

The structure in Figure 1c,i is indeed the well-known lepidocrocite type,³⁵ which is constructed by octahedral block. For a single cell, the lattice parameters are $a = 3.028$ Å and $b = 3.765$ Å and the thickness is $d = 4.33$ Å (it is the distance between atoms with the Cartesian z component maximum and minimum). The lattice parameters a and b are very close to the calculated $a = 3.029$ Å and $b = 3.733$ Å²¹ and the experimental $a = 3.0$ Å and $b = 3.8$ Å.^{19,23} The monolayer in Figure 1c,ii is formed by Ti–O hexahedral block. The lattice parameters are $a = 3.258$ Å, $b = 3.863$ Å, and $d = 4.178$ Å. The one in Figure 1c,iii is constructed by the pentahedral block. For single cell, the lattice parameters are $a = 3.016$ Å, $b = 5.101$ Å, and $d = 1.990$ Å. The one in Figure 1c,iv is constructed by tetrahedral block. For

single cell, its lattice parameters are $a = 3.233 \text{ \AA}$, $b = 5.538 \text{ \AA}$, and $d = 2.762 \text{ \AA}$.

For a monolayer composed by different polyhedral blocks, the ranking of thermal stability is: octahedral monolayer (o-ML, α phase) > hexahedral monolayer (h-ML, β phase) > tetrahedral monolayer (t-ML, δ phase) > pentahedral monolayer (p-ML, γ phase) and their thicknesses are in the same order. Excluding MLs with the lowest enthalpy discussed above, there are usually other phases for ML with the same polyhedral block. For example, there are δ' phase and δ'' phase for t-ML; their enthalpies are -8.604 and -8.219 eV/atom. The structure, thickness, and enthalpy of the four freestanding MLs formed by single polyhedral block are concluded in Table 1.

In physical insight, a stable structure must be in an energy valley.³⁶ To investigate the dynamics stability of the four structures shown in Figure 1c, phonon dispersion spectrum and density of state (DOS) were calculated by DFPT and the results are shown in Figure 2; the phonon modes and frequencies at the center of the Brillouin zone are displayed in Table 2 with the infrared activity (IR) or Raman activity (R) marked. Except t-ML, other three MLs are found to be thermodynamically stable. Because of the lack of coedge for the tetrahedral ML, the structure is highly deformable; imaginary phonon modes were found in all phases of t-ML. Therefore, only the stable ML will be discussed in the following text. It is also interesting to find that the layered structures are phononic crystals,^{37,38} e.g., there are full band gaps in the range of $406.6\text{--}421.6 \text{ cm}^{-1}$ for o-ML (α phase) and in the range of $585.9\text{--}636.8 \text{ cm}^{-1}$ for h-ML (β phase). Meanwhile, partial band gap can be found in $X \rightarrow M$, $G \rightarrow M$, or $G \rightarrow X$ direction. Because it is nonplanar compared with planar honeycomb, the DOS of 2D titania nanosheets presents less 2D characters compared with h-BN;³⁹ some steps indicating 2D features can also be found in the range of $0\text{--}100 \text{ cm}^{-1}$ for o-ML and $160\text{--}318 \text{ cm}^{-1}$ for p-ML, although they are far away from those for a strict 2D system.^{40–42}

Excluding negative frequency modes of t-ML in Figure 2 and Table 2, all modes are in the frequency range of $0\text{--}1000 \text{ cm}^{-1}$ and the ranges of o-ML, h-ML, and p-ML are very close to each other. Physically, this indicates alike interaction between atoms, which is accordant with the fact that the average enthalpies per atom are close to each other in the previous calculation.²⁷ IR modes in Table 2 contribute to the dielectric constant of nanosheet,^{28,43} whereas the Raman active mode can be used for materials detection.⁴⁴ There is no symmetric center for p-ML and t-ML; therefore, their vibration modes own both IR activity and Raman activity simultaneously.

To check the stability of monolayers in ambient temperature, AIMD simulations were performed. The fluctuation of temperature, enthalpy, and free energy during the molecular dynamics simulations as well as the final configuration are displayed in Figure 3. According to these plots, all systems quickly reach equilibrium in less than 1 ps,^{45,46} due to high thermal conductivity in a two-dimensional system.⁴⁴ The average temperatures in the last 1 ps are 300.83, 300.59, and 299.71 K, respectively, which are very close to the target temperature. After 8 ps, no structure destruction was found for α phase o-ML, β phase h-ML, and γ phase p-ML. Actually, the energy differences between the neighboring phases listed in Figure 1 are $\sim 100\text{--}300 \text{ meV/atom}$, which is much larger than the thermal vibration energy corresponding to room temperature ($\sim 26 \text{ meV}$, 300 K). The phase change always involves the bond reconstruction, which is not likely to happen at ambient temperature.

To interpret these electron relevant properties, electron band structure and partial density of state (PDOS) are calculated and shown in Figure 4 and Table 3. Compared with HSE06, PBE

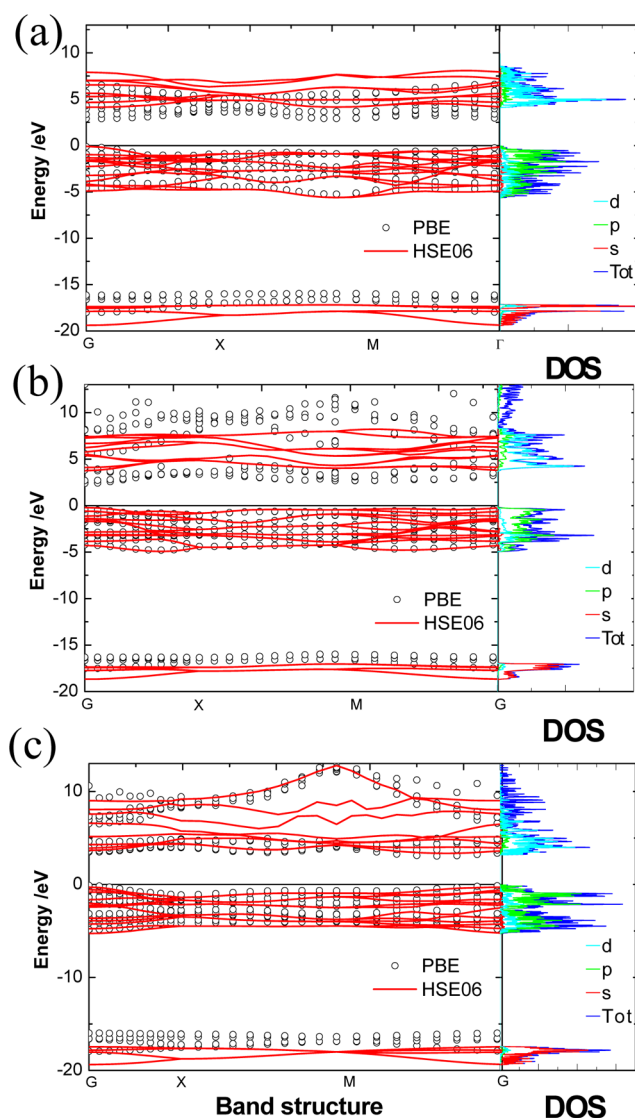


Figure 4. Electronic band structure and partial wave density of state (PDOS) of TiO_2 o-ML (α phase) (a); TiO_2 h-ML (β phase) (b); and TiO_2 p-ML (γ phase) (c). The Fermi level of the band and PDOS are set to 0 eV; Gaussian smearing: 0.01 eV.

underestimates band gap by $\sim 10\text{--}40\%$ as usual. The three kinds of monolayers are wide-gap semiconductors with band gaps larger than 3 eV; meanwhile, they are direct band gap semiconductors. The band gaps of TiO_2 2D layer are larger than those of anatase nanoparticle (3.2 eV),⁴⁷ thin film (30–40 nm, 3.2 eV),⁴⁸ and bulk (3.2 eV)⁴⁹ due to thinner structure. The band gap of o-ML 4.22 eV (HSE06) is larger than the experimental value 3.84 eV⁵⁰ probably due to defect-induced band gap narrowing in experiment.^{51,52} According to the hybrid functional calculations (HSE06), the band gap ranking is o-ML (α phase) > h-ML (β phase) > p-ML (γ phase). The wider band gaps than those of anatase and rutile TiO_2 caused by quantum-confinement effects indicate their better insulating properties than those of bulk materials. The band gap indirect–direct transition from bulk anatase TiO_2 to lepidocrocite type is also helpful for

Table 3. Valence Band Maximum (VBM), Conduction Band Bottom (CBM) Referenced to Vacuum Level, i.e., Ionization Potentials (IPs) and Electron Affinities (EAs); Band Gap of TiO₂ Monolayers with Different Polyhedral Blocks Calculated by PBE and HSE06 in Electronvolts

	o-ML (α phase)			h-ML (β phase)			p-ML (γ phase)		
	IP	EA	E_g	IP	EA	E_g	IP	EA	E_g
PBE	-8.22	-5.21	3.01	-6.65	-4.01	2.64	-7.19	-4.03	3.16
HSE06	-9.05	-4.83	4.22	-7.67	-3.83	3.84	-7.81	-4.52	3.29

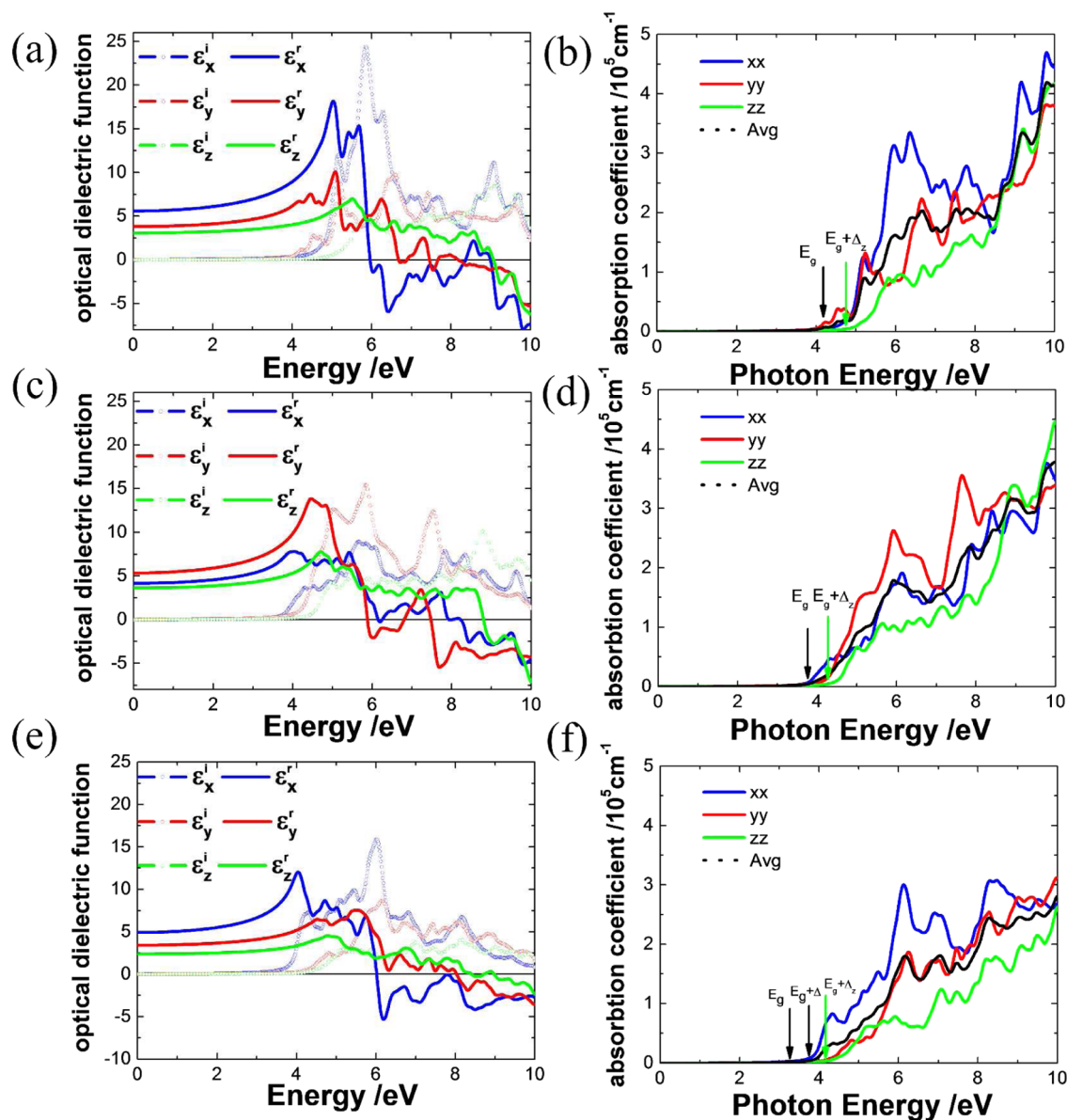


Figure 5. Optical dielectric function and photon absorption coefficient of TiO₂ o-ML (α phase) (a, b); TiO₂ h-ML (β phase) (c, d); and TiO₂ p-ML (γ phase) (e, f).

electron transition between the conduction band and valence band (VB) as well as photon absorption.⁵³ For o-ML, h-ML, and p-ML, the first valence band near the Fermi level spreads in the range ~ 0 – 1.02 , 0 – 0.707 , and 0 – 1.41 eV, respectively. The smooth curves and narrow ranges indicate it is localized, and heavy electrons in the valence band may also explain the weak near-band optical absorption⁵³ (Figure 5).

Figure 5a,c,e shows the optical dielectric functions of the three structures calculated on the basis of HSE06. The correction was done to subtract the vacuum effect according to the dielectric

equation for complex layered materials.^{21,39} Electronic screening properties are described by the complex dielectric function $\epsilon(\omega) = \epsilon_r(\omega) + i\epsilon_i(\omega)$, which depicts the electronic response to perturbation of the alternative electric field with frequency ω , and ϵ_r and ϵ_i represent screening ability of electrons and dielectric loss (photon absorption), respectively. For all sheets, the weakest screening ability is in z direction due to their size. The optical absorption onset ($\epsilon_i \neq 0$) occurs at the photon energy $\hbar\omega \approx E_g$ for direct band gap.⁵³ For the photon energy $\hbar\omega$, from 0 eV to E_g , the real dielectric constant ϵ_r of o-ML is

comparable to that of h-ML but larger than that of p-ML due to complex factors of structure, thickness, and band gap.

According to equation $A(\omega) = (\sqrt{2})\omega[\sqrt{\epsilon_r^2 + \epsilon_i^2} - \epsilon_r]^{1/2}$,⁵⁴ the more intuitive and experimentally available photon absorption coefficients are derived from dielectric functions and displayed in Figure 5b,d,f too. It is interesting to find that the optical absorption onset is below, equal to, and above the band gap energy, respectively, for o-ML, h-ML, and p-ML, whereas in bulk anatase and rutile, it is always above the band gap energy.⁵³ For o-ML, transitions are symmetrically allowed between CBM and VBM. Although excitons open the band gap, they extend the absorption edge to a position lower than that of E_g too. For p-ML, transitions between CBM and VBM are symmetry forbidden; VBM of the second VB is -0.5539 eV, which is just the energy difference Δ . Anisotropy of optical absorption is obvious for all sheets; it originates from their asymmetry structures, especially in z direction, where the largest Δ_z and the weakest absorption indicate strong quantum-confined effects.

Alignment of band edge to the vacuum level is important for the applications of semiconductor in heterojunction, photocatalysis, etc. Figure 6 (see Table 3 also) shows the comparison

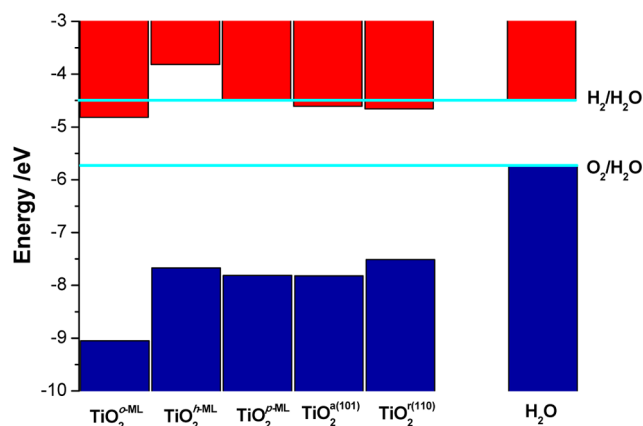


Figure 6. Calculated ionization potentials and electron affinities of TiO₂ octahedral monolayer (o-ML, α phase), hexahedral monolayer (h-ML, β phase), pentahedral monolayer (p-ML, γ phase), anatase (101) surface, and rutile (110) surface; the splitting energy of H₂O (pH = 0, 1 atm, 298 K) is shown also.

of ionization potentials and electron affinities of several TiO₂ structures, where anatase (101) surface⁵⁵ and rutile (110) surface⁵⁵ are also displayed. Accordingly, EAs of these structures are around the energy level of H⁺/H₂ redox couple (-4.5 eV)⁵⁵ but exclude h-ML, which is 0.67 eV higher and EA of p-ML is slightly lower (0.02 eV); others are ~ 0.33 eV lower. And their IPs are all lower than the energy level of OH⁻/O₂ redox couple (-5.73 eV).⁵⁵ According to the band alignment, they all can be applied in photolysis (water, organic molecules, etc.)^{55–57} and the electrons in the conduction band edge of h-ML have the strongest reducibility and holes in o-ML own the strongest oxidizability from pure energy perspective.

4. CONCLUSIONS

The structures of TiO₂ monolayer were studied by evolution algorithm, which can be composed by Ti–O block of octahedron (α phase), hexahedron (β phase), pentahedron (γ phase), and tetrahedron (δ phase). The order of their enthalpies

was found to be: o-ML (α phase) < h-ML (β phase) < t-ML (δ phase) < p-ML (γ phase), except δ phase; other phases are thermodynamically stable; the lepidocrocite type (α phase) sheet is proved to be the most stable freestanding two-dimensional TiO₂. Meanwhile, structure-dependent properties were studied by ab initio calculation. The layered structures are full or partial band gaps in a phonon spectrum so can be used as phononic crystals. They are direct band gap semiconductors with a wide gap larger than 3 eV by HSE06. The order for band gaps as well as thickness are o-ML (α phase) > h-ML (β phase) > p-ML (γ phase). Better insulation property is expected for the layered structure compared with bulk. Abnormal optical absorption compared with bulk titania was observed. And the strongest photocatalysis reducibility and oxidizability were found in the h-ML and o-ML structure, respectively.

AUTHOR INFORMATION

Corresponding Author

*E-mail: wangliang@cigit.ac.cn.

ORCID

Liang Wang: 0000-0002-6712-6500

Notes

The authors declare no competing financial interest.

ACKNOWLEDGMENTS

This work was supported by the program of Hundred talents of Chinese Academy of Sciences (Grant no. R52A261Z10) and the Fundamental and Advanced Technology Research Funds of Chongqing (Grant no. cstc2015jcyjbx0103). Authors would like to thank National Supercomputer Center in Guangzhou for supplying calculation resource of MILKYWAY-2-TH-IVB-FEP cluster.

REFERENCES

- Osada, M.; Sasaki, T. Two-Dimensional Dielectric Nanosheets: Novel Nanoelectronics from Nanocrystal Building Blocks. *Adv. Mater.* **2012**, *24*, 210–228.
- Kim, Y. H.; Dong, L.; Osada, M.; Li, B. W.; Ebina, Y.; Sasaki, T. Artificial Design for New Ferroelectrics Using Nanosheet-Architectonics Concept. *Nanotechnology* **2015**, *26*, No. 244001.
- Tuichai, W.; Thongyong, N.; Danwittayakul, S.; Chanlek, N.; Srepusharawoot, P.; Thongbai, P.; Maensiri, S. Very Low Dielectric Loss and Giant Dielectric Response with Excellent Temperature Stability of Ga³⁺ and Ta⁵⁺ Co-Doped Rutile-TiO₂ Ceramics. *Mater. Des.* **2017**, *123*, 15–23.
- Umari, P.; Giacomazzi, L.; De Angelis, F.; Pastore, M.; Baroni, S. Energy-Level Alignment in Organic Dye-Sensitized TiO₂ from Gw Calculations. *J. Chem. Phys.* **2013**, *139*, No. 014709.
- Yuan, J. J.; Li, H. D.; Wang, Q. L.; Yu, Q.; Zhang, X. K.; Yu, H. J.; Xie, Y. M. Fabrication, Characterization, and Photocatalytic Activity of Double-Layer TiO₂ Nanosheet Films. *Mater. Lett.* **2012**, *81*, 123–126.
- Hamdi, A.; Boussekey, L.; Roussel, P.; Addad, A.; Ezzaouia, H.; Boukherroub, R.; Coffinier, Y. Hydrothermal Preparation of MoS₂/TiO₂/Si Nanowires Composite with Enhanced Photocatalytic Performance under Visible Light. *Mater. Des.* **2016**, *109*, 634–643.
- Al-Khatatbeh, Y.; Lee, K. K. M.; Kiefer, B. High-Pressure Behavior of TiO₂ as Determined by Experiment and Theory. *Phys. Rev. B* **2009**, *79*, No. 134114.
- Popescu, C.; Angel Sans, J.; Errandonea, D.; Segura, A.; Villanueva, R.; Sapina, F. Compressibility and Structural Stability of Nanocrystalline TiO₂ Anatase Synthesized from Freeze-Dried Precursors. *Inorg. Chem.* **2014**, *53*, 11598–11603.
- Chen, Y. I. *Nanotubes and Nanosheets: Functionalization and Applications of Boron Nitride and Other Nanomaterials*; CRC Press: Boca Raton, 2015.

- (10) Ali, M. A. N. *Two-Dimensional Nanostructures*; Taylor & Francis: Boca Raton, 2012.
- (11) Zheng, H.; Li, X.-B.; Chen, N.-K.; Xie, S.-Y.; Tian, W. Q.; Chen, Y.; Xia, H.; Zhang, S. B.; Sun, H.-B. Monolayer II-VI Semiconductors: A First-Principles Prediction. *Phys. Rev. B* **2015**, *92*, No. 115307.
- (12) Song, T. T.; et al. The Stability of Aluminium Oxide Monolayer and Its Interface with Two-Dimensional Materials. *Sci. Rep.* **2016**, *6*, No. 29221.
- (13) Yin, K.; Zhang, Y.-Y.; Zhou, Y.; Sun, L.; Chisholm, M. F.; Pantelides, S. T.; Zhou, W. Unsupported Single-Atom-Thick Copper Oxide Monolayers. *2d Mater.* **2017**, *4*, No. 011001.
- (14) Tang, Q.; Zhou, Z.; Chen, Z. F. Innovation and Discovery of Graphene-Like Materials Via Density-Functional Theory Computations. *Wiley Interdiscip. Rev.: Comput. Mol. Sci.* **2015**, *5*, 360–379.
- (15) Masuda, Y.; Giorgi, G.; Yamashita, K. DFT Study of Anatase-Derived TiO₂ Nanosheets/Graphene Hybrid Materials. *Phys. Status Solidi B* **2014**, *251*, 1471–1479.
- (16) Zhang, H. Ultrathin Two-Dimensional Nanomaterials. *ACS Nano* **2015**, *9*, 9451–9469.
- (17) Geng, F.; Renzhi, M.; Nakamura, A.; Akatsuka, K.; Ebina, Y.; Yamauchi, Y.; Miyamoto, N.; Tateyama, Y.; Sasaki, T. Unusually Stable ~100-Fold Reversible and Instantaneous Swelling of Inorganic Layered Materials. *Nat. Commun.* **2013**, *4*, No. 1632.
- (18) Ohwada, M.; Kimoto, K.; Mizoguchi, T.; Ebina, Y.; Sasaki, T. Atomic Structure of Titania Nanosheet with Vacancies. *Sci. Rep.* **2013**, *3*, No. 2801.
- (19) Wang, Y.; Sun, C. H.; Yan, X. X.; Xiu, F. X.; Wang, L. Z.; Smith, S. C.; Wang, K. L.; Lu, G. Q.; Zou, J. Lattice Distortion Oriented Angular Self-Assembly of Monolayer Titania Sheets. *J. Am. Chem. Soc.* **2011**, *133*, 695–697.
- (20) Sasaki, T.; Watanabe, M.; Hashizume, H.; Yamada, H.; Nakazawa, H. Macromolecule-Like Aspects for a Colloidal Suspension of an Exfoliated Titanate. Pairwise Association of Nanosheets and Dynamic Reassembling Process Initiated from It. *J. Am. Chem. Soc.* **1996**, *118*, 8329–8335.
- (21) Sato, H.; Ono, K.; Sasaki, T.; Yamagishi, A. First-Principles Study of Two-Dimensional Titanium Dioxides. *J. Phys. Chem. B* **2003**, *107*, 9824–9828.
- (22) Sasaki, T.; Watanabe, M. Osmotic Swelling to Exfoliation. Exceptionally High Degrees of Hydration of a Layered Titanate. *J. Am. Chem. Soc.* **1998**, *120*, 4682–4689.
- (23) Tanaka, T.; Ebina, Y.; Takada, K.; Kurashima, K.; Sasaki, T. Oversized Titania Nanosheet Crystallites Derived from Flux-Grown Layered Titanate Single Crystals. *Chem. Mater.* **2003**, *15*, 3564–3568.
- (24) Glass, C. W.; Oganov, A. R.; Hansen, N. Uspex - Evolutionary Crystal Structure Prediction. *Comput. Phys. Commun.* **2006**, *175*, 713–720.
- (25) Kresse, G.; Furthmüller, J. Efficiency of Ab-Initio Total Energy Calculations for Metals and Semiconductors Using a Plane-Wave Basis Set. *Comput. Mater. Sci.* **1996**, *6*, 15–50.
- (26) Kresse, G.; Furthmüller, J. Efficient Iterative Schemes for Ab Initio Total-Energy Calculations Using a Plane-Wave Basis Set. *Phys. Rev. B* **1996**, *54*, 11169–11186.
- (27) Blöchl, P. E. Projector Augmented-Wave Method. *Phys. Rev. B* **1994**, *50*, 17953–17979.
- (28) Baroni, S.; de Gironcoli, S.; Dal Corso, A.; Giannozzi, P. Phonons and Related Crystal Properties from Density-Functional Perturbation Theory. *Rev. Mod. Phys.* **2001**, *73*, 515–562.
- (29) Perdew, J. P.; Burke, K.; Ernzerhof, M. Generalized Gradient Approximation Made Simple. *Phys. Rev. Lett.* **1996**, *77*, 3865–3868.
- (30) Monkhorst, H. J.; Pack, J. D. Special Points for Brillouin-Zone Integrations. *Phys. Rev. B* **1976**, *13*, 5188–5192.
- (31) Heyd, J.; Scuseria, G. E.; Ernzerhof, M. Hybrid Functionals Based on a Screened Coulomb Potential. *J. Chem. Phys.* **2003**, *118*, 8207–8215.
- (32) Heyd, J.; Scuseria, G. E.; Ernzerhof, M. Hybrid Functionals Based on a Screened Coulomb Potential. *J. Chem. Phys.* **2006**, *124*, No. 219906.
- (33) Nosé, S. A Unified Formulation of the Constant Temperature Molecular-Dynamics Methods. *J. Chem. Phys.* **1984**, *81*, 511–519.
- (34) Giannozzi, P.; et al. Quantum Espresso: A Modular and Open-Source Software Project for Quantum Simulations of Materials. *J. Phys.: Condens. Matter* **2009**, *21*, No. 395502.
- (35) Lee, K.; Mazare, A.; Schmuki, P. One-Dimensional Titanium Dioxide Nanomaterials: Nanotubes. *Chem. Rev.* **2014**, *114*, 9385–9454.
- (36) Oganov, A. R.; Valle, M. How to Quantify Energy Landscapes of Solids. *J. Chem. Phys.* **2009**, *130*, No. 104504.
- (37) Hur, K.; Hennig, R. G.; Wiesner, U. Exploring Periodic Bicontinuous Cubic Network Structures with Complete Phononic Bandgaps. *J. Phys. Chem. C* **2017**, *121*, 22347–22352.
- (38) Zanjan, M. B.; Lukes, J. R. Shape- and Structure-Based Phonon Bandgap Tuning with Nanocrystal Superlattices. *J. Phys. Chem. C* **2015**, *119*, 16889–16896.
- (39) Wang, L.; Pu, Y. Y.; Soh, A. K.; Shi, Y. P.; Liu, S. Y. Layers Dependent Dielectric Properties of Two Dimensional Hexagonal Boron Nitride Nanosheets. *AIP Adv.* **2016**, *6*, No. 125126.
- (40) Xie, J. L.; Guo, C. X.; Li, C. M. Construction of One-Dimensional Nanostructures on Graphene for Efficient Energy Conversion and Storage. *Energy Environ. Sci.* **2014**, *7*, 2559–2579.
- (41) Balandin, A. Thermal Properties of Semiconductor Low-Dimensional Structures. *Phys. Low-Dimens. Struct.* **2000**, *1–2*, 1–28.
- (42) Alofi, A.; Srivastava, G. P. Thermal Conductivity of Graphene and Graphite. *Phys. Rev. B* **2013**, *87*, No. 115421.
- (43) Schöche, S.; Hofmann, T.; Korlacki, R.; Tiwald, T. E.; Schubert, M. Infrared Dielectric Anisotropy and Phonon Modes of Rutile TiO₂. *J. Appl. Phys.* **2013**, *113*, No. 164102.
- (44) Xu, X.; Chen, J.; Li, B. W. Phonon Thermal Conduction in Novel 2d Materials. *J. Phys.: Condens. Matter* **2016**, *28*, No. 483001.
- (45) Du, A.; Sanvito, S.; Smith, S. C. First-Principles Prediction of Metal-Free Magnetism and Intrinsic Half-Metallicity in Graphitic Carbon Nitride. *Phys. Rev. Lett.* **2012**, *108*, No. 197207.
- (46) Xu, B.; Yin, J.; Xia, Y. D.; Wan, X. G.; Jiang, K.; Liu, Z. G. Electronic and Magnetic Properties of Zigzag Graphene Nanoribbon with One Edge Saturated. *Appl. Phys. Lett.* **2010**, *96*, No. 163102.
- (47) Scanlon, D. O.; et al. Band Alignment of Rutile and Anatase TiO₂. *Nat. Mater.* **2013**, *12*, 798–801.
- (48) Tang, H.; Prasad, K.; Sanjines, R.; Schmid, P. E.; Levy, F. Electrical and Optical-Properties of TiO₂ Anatase Thin-Films. *J. Appl. Phys.* **1994**, *75*, 2042–2047.
- (49) Tang, H.; Levy, F.; Berger, H.; Schmid, P. E. Urbach Tail of Anatase TiO₂. *Phys. Rev. B* **1995**, *52*, 7771–7774.
- (50) Sakai, N.; Ebina, Y.; Takada, K.; Sasaki, T. Electronic Band Structure of Titania Semiconductor Nanosheets Revealed by Electrochemical and Photoelectrochemical Studies. *J. Am. Chem. Soc.* **2004**, *126*, 5851–5858.
- (51) Guo, X.; Zheng, H.; King, S. W.; Afanas'ev, V. V.; Baklanov, M. R.; de Marneffe, J. F.; Nishi, Y.; Shohet, J. L. Defect-Induced Bandgap Narrowing in Low-K Dielectrics. *Appl. Phys. Lett.* **2015**, *107*, No. 082903.
- (52) Kamble, V. B.; Umarji, A. M. Defect Induced Optical Bandgap Narrowing in Undoped SnO₂ Nanocrystals. *AIP Adv.* **2013**, *3*, No. 082120.
- (53) Dou, M.; Persson, C. Comparative Study of Rutile and Anatase SnO₂ and TiO₂: Band-Edge Structures, Dielectric Functions, and Polaron Effects. *J. Appl. Phys.* **2013**, *113*, No. 083703.
- (54) Shi, H.; Chu, M.; Zhang, P. Optical Properties of UO₂ and PuO₂. *J. Nucl. Mater.* **2010**, *400*, 151–156.
- (55) Stevanović, V.; Lany, S.; Ginley, D. S.; Tumas, W.; Zunger, A. Assessing Capability of Semiconductors to Split Water Using Ionization Potentials and Electron Affinities Only. *Phys. Chem. Chem. Phys.* **2014**, *16*, 3706–3714.
- (56) Wang, Y.; Mo, Z.; Zhang, P.; Zhang, C.; Han, L.; Guo, R.; Gou, H.; Wei, X.; Hu, R. Synthesis of Flower-Like TiO₂ Microsphere/Graphene Composite for Removal of Organic Dye from Water. *Mater. Des.* **2016**, *99*, 378–388.

(57) Yang, Y.; Xu, L.; Wang, H.; Wang, W.; Zhang, L. TiO₂/Graphene Porous Composite and Its Photocatalytic Degradation of Methylene Blue. *Mater. Des.* **2016**, *108*, 632–639.